

HVDistill: Transferring Knowledge from Images to Point Clouds via Unsupervised Hybrid-View Distillation

Sha Zhang^{1,3} · Jiajun Deng² · Lei Bai³ · Houqiang Li¹ · Wanli Ouyang³ · Yanyong Zhang¹

Received: date / Accepted: date

Abstract We present a hybrid-view-based knowledge distillation framework, termed HVDistill, to guide the feature learning of a point cloud neural network with a pre-trained image network in an unsupervised manner. By exploiting the geometric relationship between RGB cameras and LiDAR sensors, the correspondence between the two modalities based on both image-plane view and bird-eye view can be established, which facilitates representation learning. Specifically, the image-plane correspondences can be simply obtained by projecting the point clouds, while the bird-eye-view correspondences can be achieved by lifting the pixels to the 3D space with the predicted depths under the supervision of projected point clouds. The image teacher networks provide rich semantics from the image-plane view and meanwhile acquire geometric information from the bird-eye view. Indeed, im-

age features from the two views naturally complement each other and together can ameliorate the learned feature representation of the point cloud student networks. Moreover, with a self-supervised pre-trained 2D network, HVDistill requires neither 2D nor 3D annotations. We pre-train our model on nuScenes dataset and transfer it to several downstream tasks on nuScenes, SemanticKITTI, and KITTI datasets for evaluation. Extensive experimental results show that our method achieves consistent improvements over the baseline trained from scratch and significantly outperforms the existing schemes. Codes are available at [git@github.com:zhangsha1024/HVDistill.git](https://github.com:zhangsha1024/HVDistill.git).

Keywords unsupervised learning · representation learning · cross-modal distillation · point clouds representation learning

Sha Zhang
E-mail: zhsh1@mail.ustc.edu.cn

Jiajun Deng, corresponding author
E-mail: jiajun.deng@adelaide.edu.au

Lei Bai
E-mail: baisanshi@gmail.com

Houqiang Li
E-mail: lihq@ustc.edu.cn

Wanli Ouyang
E-mail: wanli.ouyang@sydney.edu.au

Yanyong Zhang, corresponding author
E-mail: yanyongz@ustc.edu.cn

¹University of Science and Technology of China, Hefei, Anhui, China

²The University of Adelaide, Adelaide, Australia

³Shanghai AI Laboratory, Shanghai, China

1 Introduction

LiDAR point clouds play a vital role in 3D perception for numerous applications, such as autonomous driving (Zhu et al. 2022; Li et al. 2022a; Wang et al. 2023), virtual reality (Han et al. 2021a; Alexiou et al. 2020), and domestic robotics (Qi et al. 2020; Duan et al. 2022), etc. However, collecting and annotating point clouds incur prohibitive costs (Behley et al. 2019; Caesar et al. 2020), limiting both the quantity and quality of the available datasets to date. The pretrain-and-finetune paradigm, which has achieved inspiring successes on 2D images, cannot be directly applied to the 3D domain. As a result, the previously developed point cloud processing models are generally initialized from scratch and trained with an enormous amount of samples (Shi et al. 2023). The absence of a properly pretrained model has thus become one of the major stumbling blocks in the

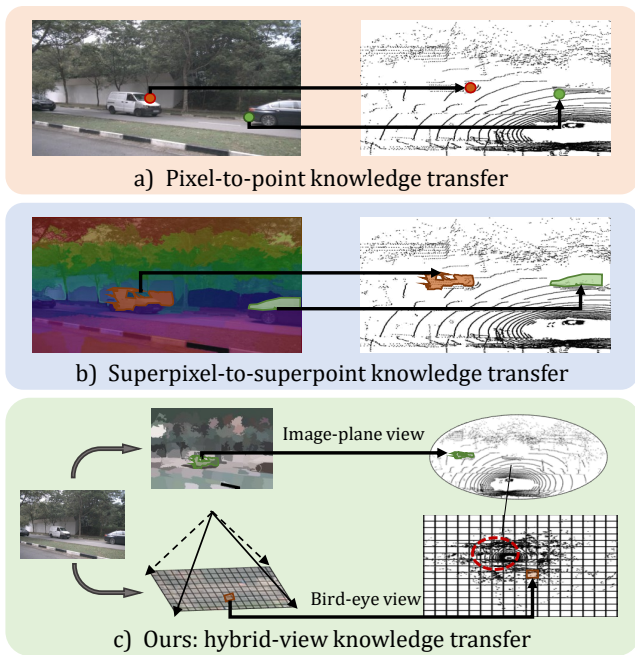


Fig. 1: Comparison between existing schemes and ours. Both (a) and (b) transfer image knowledge to point cloud networks based on the image-plane view. In contrast, we develop a hybrid-view framework (c) to transfer image knowledge based on both the image-plane view and the bird-eye view.

3D perception field (Xie et al. 2020; Liu et al. 2021a; Sautier et al. 2022).

In fact, neural networks can learn from unsupervised pretext tasks with a carefully designed loss function (He et al. 2022; Grill et al. 2020; He et al. 2020), which is known as unsupervised feature learning (UFL). In 2D image domain, UFL has been validated to be extremely effective in providing powerful and transferable feature representation for various downstream tasks (Xiao et al. 2022; Xie et al. 2022). However, when it comes to 3D point clouds, UFL hasn’t shown such impact. The main reason is that the success in images is based on millions or even billions of training samples, while datasets at such scale are unavailable for point clouds. Besides, compared to image pixels, LiDAR points are sparse and unevenly distributed, rendering it harder to learn the appropriate feature representations.

Alternatively, the properly calibrated images and point clouds that are often available for autonomous vehicles can provide a potential solution to transfer knowledge learned from images to point clouds in a cross-modality manner. As shown in Figure 1(a), the early work PPKT (Liu et al. 2021a) performs 2D-to-3D knowledge transfer via pixel-to-point contrastive learning. However, the pixel-to-point correspondence needed

by this approach is imperfect in autonomous driving scenes due to issues such as sensor occlusion and motion blur. To address this problem, the more recent work SLidR (Sautier et al. 2022) proposes to use superpixels and superpoints instead for more reliable cross-modal correspondences. As illustrated in Figure 1(b), SLidR first groups visually similar pixels into superpixels, and then performs 2D-to-3D knowledge transfer via contrastive loss between superpixels and superpoints. Here, a superpoint indicates a set of points projected to the same superpixel.

These prior studies attempt to learn point cloud representation from an image teacher network by developing 2D-3D correspondences based on the image-plane view (IPV). However, images are inherently insufficient to represent 3D scenes due to the unavailability of 3D geometric information. As such, the 2D features extracted from the IPV alone naturally fall short in guiding the representation learning of a point cloud network, taking risks in ignoring 3D spatial layouts. In this paper, we strive to enhance the 2D-to-3D knowledge transfer by also considering the 2D features from other views that can be derived from images. Formally, we introduce a hybrid-view framework, termed HVDistill, to distill image knowledge to point cloud networks in an unsupervised manner. As shown in Figure 1(c), in addition to IPV, our HVDistill further leverages the bird-eye view (BEV) as a complement for knowledge transferring. As such, the usage of both the image-plane view and bird-eye view yields a virtual 3D space, from which better 3D representations can be learned, with both semantic and geometric information taken into consideration.

The most notable design consideration of HVDistill is the addition of the image’s BEV features. Specifically, when projecting 3D points to the image plane as in previous methods (Liu et al. 2021a; Sautier et al. 2022), we not only build the correspondences between points and pixels but also obtain the depth information for the pixels with projected points. However, due to the sparsity of point clouds, only a small fraction of pixels has direct correspondences with points, which means huge potential untapped. In our algorithm, we address this issue by estimating a dense depth map for each image under the supervision of the sparse depth map directly provided by point clouds. We combine the image features with camera intrinsic to estimate the depth for

each pixel. Once obtaining the depth, the pixels can be “lifted” to the 3D space (Wang et al. 2019). Next, we splat the lifted pixels to the BEV plane, because the BEV representation has been validated to be effective in 3D perception tasks for autonomous driving (Liu et al. 2022; Huang et al. 2021; Li et al. 2022b), where the objects are not likely to overlap with each other and their sizes are consistent with the real world ignoring the distance to the ego sensor.

To validate the merits of our proposed framework, we first conduct pre-training on nuScenes dataset (Caesar et al. 2020), and then evaluate the learned representation on two typical 3D perception tasks, *i.e.*, 3D semantic segmentation and 3D object detection, over three prevalent benchmarks, *i.e.*, nuScenes-Lidarseg (Caesar et al. 2020), SemanticKITTI (Behley et al. 2019) and KITTI (Geiger et al. 2012). Our HVDistill achieves improvements on all three datasets. Remarkably, the model pre-trained with HVDistill achieves 49.7% mIoU, resulting in 5.1% performance improvement over the strongest counterpart for few-shot semantic segmentation on SemanticKITTI, and up to 8.7% mAP improvements for few-shot object detection.

In summary, our main contribution is the HVDistill framework that transfers image knowledge to point cloud networks via cross-modality contrastive distillation based on image-plane and bird-eye views. Compared to prior works, the hybrid-view image teachers in our HVDistill take both semantic and geometric information into account, thus learning the effective representation from point clouds. Moreover, we provide an elegant solution to involve the image’s BEV features with marginal cost and no extra annotations. Our HVDistill takes a strong step towards effective pre-trained networks for 3D point clouds and exhibits great potential to serve as a baseline for future investigation.

2 Related Work

In this section, we briefly review unsupervised feature learning (UFL) and cross-modality knowledge distillation.

2.1 UFL for Point Clouds

Unsupervised feature learning aims to learn general feature representation without human-annotated labels. The learned representation is supposed to be easily adapted to downstream tasks via fine-tuning.

The existing intra-modality UFL methods for point clouds can be divided into two categories: generative-based methods and contrastive-based methods.

Generative-based methods (Han et al. 2019a, 2021b; Chen et al. 2021; Han et al. 2019b; Rao et al. 2020; Chen et al. 2019; Zhao et al. 2022b), explore 3D data reconstruction as pretext tasks to learn effective feature representation. Typically, a series of pretext tasks are involved, including 3D objects reconstruction (Chen et al. 2021; Han et al. 2019b; Zhao et al. 2022b), point clouds completion (Rao et al. 2020; Chen et al. 2019; Yang et al. 2017) and rotation prediction (Han et al. 2019a, 2021b). Besides, PC-GAN (Li et al. 2018) introduces generative adversarial networks to the point clouds domain, learning point clouds’ feature via joint distribution estimation.

Contrastive-based methods (Xie et al. 2020; Zhang et al. 2021; Wang et al. 2021; Jiang et al. 2021) follow the paradigm to learn effective point clouds features by encouraging the augmentations of the same input to approach each other while pushing away that of different inputs. Info3D (Sanghi 2020) proposes to maximize the mutual information between the whole 3D objects’ point clouds and their chunks to improve the feature representation. PointContrast (Xie et al. 2020), for the first time, generalizes self-supervised representation learning to point clouds in complex scenes by leveraging the correspondence between points from different camera views and shows that the pre-trained models can be efficiently transferred to facilitate multiple downstream tasks (e.g., classification, object detection, part segmentation, and semantic segmentation). Unlike PointContrast which relies on correspondences between points from different camera views, DepthContrast (Zhang et al. 2021) shows that performing contrastive learning with the global feature of the whole 3D scene is enough to learn effective representation.

2.2 Cross-Modality Knowledge Distillation

Knowledge distillation (KD) (Buciluă et al. 2006; Hinton et al. 2015) is first introduced to train a small model (*i.e.*, student) with the guidance of a well-performing large one (*i.e.*, teacher) for model compression. The follow-up works (Mirzadeh et al. 2020; Cho and Hariharan 2019; Zhang and Ma 2020; Zhao et al. 2022a) explore KD in various tasks and demonstrate its effectiveness in knowledge transferring, especially via a cross-modality manner (Gupta et al. 2016; Guo et al. 2021; Alwassel et al. 2020; Tian et al. 2019; Liu et al. 2021b).

Cross-modality KD has attracted increasing attention in 3D perception fields. Among the surge of re-

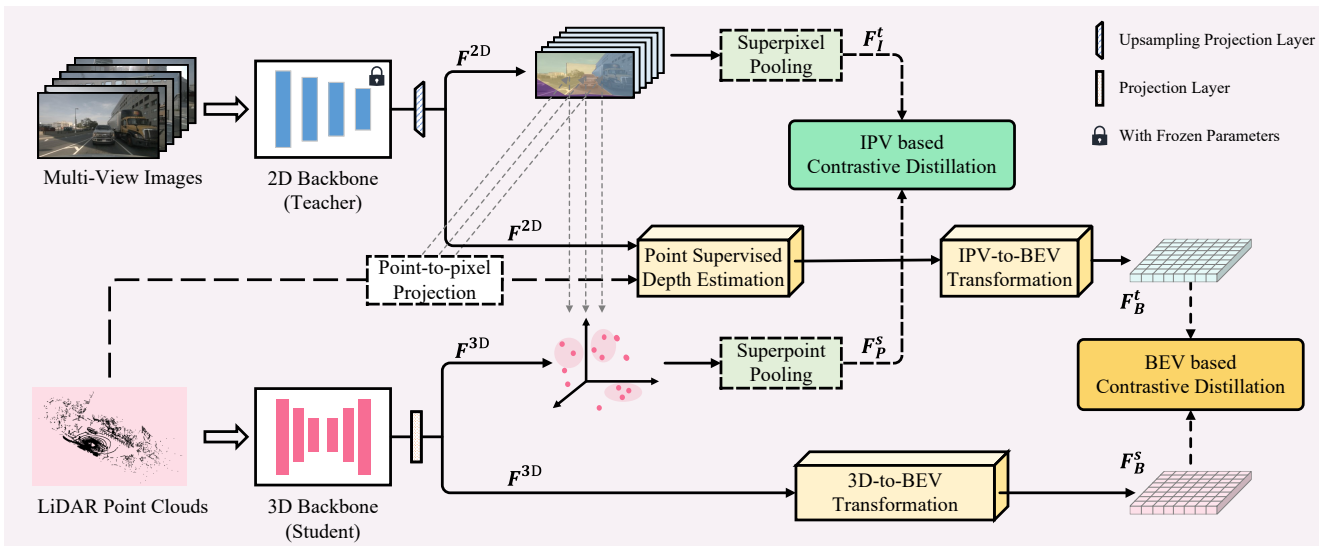


Fig. 2: **An overview of the proposed HVDistill pipeline.** Our approach transfers image knowledge from a pre-trained 2D network into a 3D neural network via hybrid-view contrastive distillation. On one hand, the point clouds are grouped into superpoints according to the corresponding superpixels generated on each image, and then supervised by the image features from the 2D teacher network by image-plane view (IPV) based contrastive distillation. On the other hand, the features of images/point clouds from 2D/3D backbones are transformed to the bird-eye view (BEV), and then the image BEV features are used for supervising the point cloud BEV features by contrastive loss. Note that the 2D backbone’s parameters are frozen.

search, several recent works (Liu et al. 2021a; Sautier et al. 2022) distill knowledge in the same setting as ours: treating a well-pretrained image model as the teacher and a randomly initialized point clouds model as the student. Specifically, PPKT (Liu et al. 2021a) optimizes the point cloud features network by mimicking the corresponding image features in a pixel-to-point manner. However, the accurate matching of pixel-to-point is not always accessible in real-world data, especially in autonomous driving, hampering the effectiveness of the learned point cloud feature. Instead, SLidR (Sautier et al. 2022) proposes to use superpixels-to-superpoints as an alternative. It groups visually similar pixels to superpixels and obtains corresponding superpoints by projection. The contrastive distillation is then performed among superpixels and superpoints.

From our point of view, these two works both conduct contrastive learning based on the correspondence of image-plane view, which is insufficient for point cloud representation learning. In contrast, we argue that BEV-level features can provide a different viewpoint and compensates for the 3D geometric information. Meanwhile, the combination of image-plane view and BEV can narrow the domain gap during 2D-to-3D distillation, achieving more excellent performance.

3 Methodology

HVDistill is an unsupervised pre-training pipeline that transfers knowledge from a pre-trained image network to a point cloud network via hybrid-view knowledge distillation.

An overview of HVDistill is depicted in Figure 2. Given paired point clouds and images, a 3D backbone network and a 2D backbone network are applied to extract 3D point cloud features and 2D image features, respectively. After that, knowledge transferring is conducted through the image-plane view (IPV) based and bird-eye view (BEV) based contrastive distillation. On the one hand, pixels are grouped into superpixels, and superpoints are generated accordingly. The feature of superpixel is obtained by average pooling over image features, and the feature of superpoint is obtained by average pooling over point cloud features. Then, IPV-based contrastive distillation is performed based on superpixels and superpoints. On the other hand, we transform image features from IPV to BEV in three steps: (1) we project points to the image plane by geometric relationship to generate a sparse depth map with accurate depth value; (2) with the supervision of the sparse depth map, we predict a dense depth map via a depth prediction head; and (3) we lift the pixel-level features

to the 3D space according to the depth and then collapse it to BEV to produce image BEV features.

The image BEV features are leveraged to supervise the point clouds BEV features by grid-to-grid BEV-based contrastive distillation.

In the following subsections, we first briefly introduce preliminary information and then present the detailed design of our hybrid-view distillation algorithm.

3.1 Preliminary

Before introducing the hybrid-view distillation framework and training objectives of HVDistill, we briefly review knowledge distillation (KD) and contrastive learning (CL) techniques, which serve as the preliminary of our work.

Knowledge Distillation (KD): The conventional target of KD is to transfer the knowledge from an unwieldy network to a smaller network. The network to provide knowledge is known as a teacher network, and the network to be learned is the student network. In this work, we follow the recent practices (Gupta et al. 2016; Guo et al. 2021; Liu et al. 2021b) to extend this conventional target to a general one. Particularly, HVDistill is intended to transfer the knowledge of 2D networks trained with images to a 3D network aiming at point clouds, learning the benefits of rich semantic information from images. We denote the 2D teacher network as $\mathcal{N}^t(\cdot)$ and the 3D student network as $\mathcal{N}^s(\cdot)$. The parameters of $\mathcal{N}^t(\cdot)$ are frozen in our method.

Contrastive Learning (CL): CL is widely adopted as a pretext task for unsupervised representation learning (He et al. 2020; Wang et al. 2021; Jiang et al. 2021), with the training objective to reduce the feature distance between positive pairs while increasing that between negative ones. Since the traditional margin-based loss function is hard to be optimized, the CL methods usually use the noise contrastive estimation loss InfoNCE (Oord et al. 2018), which is computed as follows:

$$\mathcal{L}_{\text{InfoNCE}} = -\log \frac{\exp((F_k)^T F'_k / \tau)}{\sum_{i=1}^N \exp((F_k)^T F'_i / \tau)}. \quad (1)$$

Our HVDistill follows the feature-based paradigm to perform images to point clouds KD. Knowledge is transferred via image plane view and bird-eye view with two InfoNCE loss variants in an unsupervised manner.

3.2 Hybrid-View Distillation

The primary innovation of this work is the hybrid-view contrastive distillation for point cloud network pre-

training. Given a scan of point cloud $P_0 \in \mathbb{R}^{N \times 3}$ and multi-view images $\mathcal{I} = \{I_1, I_2, \dots, I_K \mid I_i \in \mathbb{R}^{H \times W \times 3}\}$ as the inputs, our method first applies the 3D/2D backbones to extract point/image features. A high-resolution feature map is necessary for establishing point-to-pixel correspondences, while the output of the 2D backbone network (*i.e.*, ResNet) is usually overly downsampled for the correspondence. We replace the downsampling convolutional layers with dilation convolutional layers following previous methods (Sautier et al. 2022) and add an upsampling projection layer \mathcal{H}^t following the 2D backbone $\mathcal{N}^t(\cdot)$ to obtain a high-resolution image feature map $\mathbf{F}_k^{2D} \in \mathbb{R}^{H \times W \times C}$, where k indicates the k -th view. Note that the spatial resolution of \mathbf{F}_k^{2D} is the same as that of input images but with C channels. Another projection layer \mathcal{H}^s is then applied to the point features out of the 3D backbone $\mathcal{N}^s(\cdot)$ to produce point cloud features $\mathbf{F}^{3D} \in \mathbb{R}^{N \times C}$ that match the feature dimension of each \mathbf{F}_k^{2D} . Our proposed hybrid-view distillation, including IPV-based contrastive distillation and BEV-based contrastive distillation, is built on $\{\mathbf{F}_k^{2D}\}_{k=1}^K$ and \mathbf{F}^{3D} .

IPV based Contrastive Distillation: IPV-based contrastive distillation transfers knowledge from 2D backbone to 3D backbone via cross-modality contrastive learning between 2D features from the image plane and point cloud features from the 3D space. We name it IPV based since the teacher signals, *i.e.*, 2D features, are from the image plane.

Inspired by the method in (Sautier et al. 2022), we perform contrastive learning at the cluster level. Specifically, visually similar pixels in each image are grouped together to generate superpixels with a bottom-up segmentation algorithm, SLIC (Achanta et al. 2012). We use C_k^m to denote the set of pixels belonging to the m -th superpixel from the k -th image. An L2 normalization function followed by an average pooling is applied on \mathbf{F}^{2D} to produce the superpixel’s feature $\mathbf{F}_{I(k,m)}^t$ as:

$$\mathbf{F}_{I(k,m)}^t = \frac{1}{|C_k^m|} \sum_{(x,y) \in C_k^m} \frac{\mathbf{F}_k^{2D}(x,y)}{\|\mathbf{F}_k^{2D}(x,y)\|_2}, \quad (2)$$

where (x,y) is the index of a pixel in the image feature map. In the 3D space, we use superpoints as a cluster to learn from superpixels. To generate superpoints, we first obtain the point-pixel correspondence by projecting the point clouds to the image plane according to the extrinsic T_{12c} and intrinsic matrices T_{c2i} . Once the point-pixel correspondence is acquired, the points projected to the same superpixel are grouped together to formulate a superpoint D_k^m :

$$D_k^m = \mathcal{G}(T_{c2i} T_{12c} \mathcal{P}, C_k^m) \quad (3)$$

Note that the correspondence between points and pixels is independently obtained for each image, thus superpoints are different for different image views. Similar to producing features of superpixels, L2 Normalization, and an average pooling layer are applied to compute the superpixel’s feature:

$$F_{P(k,m)}^s = \frac{1}{|D_k^m|} \sum_{j \in D_k^m} \frac{\mathbf{F}^{3D}(j)}{\|\mathbf{F}^{3D}(j)\|_2}, \quad (4)$$

where j is the index of a point from the 3D features.

After obtaining features of superpixels and superpoints, we utilize superpixel-to-superpoint contrastive loss to perform point cloud feature learning. The matched superpoint-superpixel pairs are taken as positive samples, while unmatched ones are taken as negative samples. In an ideal situation, the positive samples are close to each other, while the negative samples are far away from each other. Specifically, the superpixel-to-superpoint contrastive loss is adapted based on InfoNCE loss (Oord et al. 2018), and calculated as:

$$\mathcal{L}_{IPV} = - \sum_{k,m} \log \left[\frac{E_{k,m}(k,m)}{\sum_{k',m'} E_{k,m}(k',m')} \right], \quad (5)$$

with $E_{k,m}(k',m') = \exp(\mathbf{F}_{I(k,m)}^t \mathbf{F}_{P(k',m')}^s / \tau)$,

where $\tau > 0$ is a temperature coefficient that is used to smooth the sample distribution. In this situation, the objective is to minimize the distance between the feature $F_{I(k,m)}^t$ of a superpoint and the feature $F_{P(k,m)}^s$ of the corresponding superpixel within the same image and superpixel region. At the same time, the aim is to maximize the distance between superpixel features and superpoint features that do not share the same indices or belong to different scenes.

BEV based Contrastive Distillation: BEV-based contrastive distillation provides an additional view for knowledge transfer. By transforming image features and point cloud features to BEV, a complementary pathway is created to enhance the transfer of knowledge. With the supervision of point clouds, the synthesized image BEV features can effectively preserve the geometric properties and thus ameliorate the feature learning of the 3D student network. There are two steps to obtain the image BEV features: (i) point supervised depth estimation, and (ii) IPV-to-BEV transformation.

In the first step, we reuse the correspondences established from point-to-pixel projection to obtain the depths of those pixels that have matching points. Since the LiDAR point clouds are far fewer than image pixels, the obtained depth map $\mathbf{D}_{\text{sparse}} \in \mathbb{R}^{H \times W \times 1}$ is too sparse to lift the 2D image features into 3D space.

To address this issue, we add a depth prediction head in our point-supervised depth estimation module to output a dense depth map $\mathbf{D}_{\text{dense}} \in \mathbb{R}^{H_0 \times W_0 \times T}$, each element of which represents T discrete depth ranges. Specifically, the sparse depth map $\mathbf{D}_{\text{sparse}}$ generated from point clouds is leveraged as the depth supervision. Moreover, to make the depth camera aware, we combine camera intrinsic matrices \mathbf{M} with image features to form the input of the depth prediction head. The computation of $\mathbf{D}_{\text{dense}}$ can be described as:

$$\mathbf{D}_{\text{dense}} = \mathcal{N}_D(SE(MLP(\mathbf{M}), Conv(\mathbf{F}^{2D}))), \quad (6)$$

where $\mathcal{N}_D(\cdot)$ is the depth prediction head, $SE(\cdot)$ indicates a Squeeze-and-Excitation module, and $Conv(\cdot)$ represents linear transformation with a convolutional layer. The depth prediction head consists of three Residual Blocks and a Deformable Convolution layer. We use Binary Cross Entropy for the depth loss $\mathcal{L}_{\text{depth}}$.

In the subsequent step, we lift the image features to 3D space by expanding the pixel-level features along the direction of camera rays and weighting each point feature with the corresponding response from $\mathbf{D}_{\text{dense}}$. We then group the lifted 3D features within each $r \times r$ grid in the X-Y plane together and collapse them to the BEV along the Z-axis by summation. Finally, we use an L2 Normalization layer to generate the final image BEV feature map $\mathbf{F}_B^t \in \mathbb{R}^{H_b \times W_b \times E}$. This enables us to lift the image features to 3D and generate a BEV feature map, which is a key step in our approach.

The view transformation of point cloud features from the 3D space to the BEV is more straightforward. We simply flatten the 3D point cloud features \mathbf{F}^{3D} by reshaping the features along Z-axis to the channel dimension. After that, three extra convolutional layers followed by an L2 Normalization layer are applied to obtain the point cloud BEV features $\mathbf{F}_B^s \in \mathbb{R}^{H_b \times W_b \times E}$.

The image BEV feature map \mathbf{F}_B^t and the point cloud feature map \mathbf{F}_B^s are in the unified BEV representation with the same resolution, which is naturally aligned. The feature embedding $\mathbf{F}_B^s(i,j)$ from point cloud BEV features is supposed to be similar to the corresponding grid feature $\mathbf{F}_B^t(i,j)$ from the image BEV features, and quite different from the grid features in other positions or other scenes. Based on this principle, we devise the training objective of our BEV-based contrastive distillation as:

$$\mathcal{L}_{\text{BEV}} = - \sum_{i,j} \log \left[\frac{E'_{i,j}(i,j)}{\sum_{i',j'} E'_{i,j}(i',j')} \right], \quad (7)$$

with $E'_{i,j}(i',j') = \exp(\mathbf{F}_{B(i,j)}^t \mathbf{F}_{B(i',j')}^s / \tau)$,

where $\tau > 0$ is a temperature factor. In other words, if an image BEV grid and a point BEV grid have the

same index in the BEV map for the same scene, they are positive pairs and are supposed to be close to each other in the feature space. Otherwise, they are negative pairs and are supposed to be far away from each other. In practice, we only take non-zero grids in point cloud BEV maps for training to avoid the gradient collapse problem caused by empty grids.

Overall Loss: By combining the training objectives from the IPV based, BEV based pathways, and the depth prediction module, we get the loss function:

$$\mathcal{L} = \alpha\mathcal{L}_{IPV} + \beta\mathcal{L}_{BEV} + \gamma\mathcal{L}_{depth}, \quad (8)$$

where α, β, γ are the weights of each training objective.

4 Experiments

We evaluate HVDistill pre-training method by fine-tuning and linear-probing on downstream tasks over several datasets. For pre-training, we choose a public large-scale multi-modality autonomous driving dataset, i.e., nuScenes (Caesar et al. 2020). Then we fine-tune and evaluate the pre-trained model on nuScenes, nuScenes-lidarseg (Caesar et al. 2020), SemanticKITTI (Behley et al. 2019), and KITTI (Geiger et al. 2012) for different downstream tasks separately. In this section, we present the implementation details in parts: 1) datasets and metrics used in pre-training and fine-tuning. 2) the network architecture. 3) the pre-training details. 4) the downstream experiments, including transferring to point clouds semantic segmentation and few-shot 3D object detection. 5) ablation study to validate the superiority of the design.

4.1 Datasets and Metrics

nuScenes : We conduct all the pre-train experiments on this dataset. nuScenes contains 1000 scenes with 150 for testing, 150 for validation, and others for training. The whole dataset includes approximately 1.4M camera images and 390k LIDAR sweeps. Each scene has around 40 keyframes. Every keyframe provides one scan of point cloud from the LIDAR, six images from six different cameras, and the corresponding synchronization and calibration information.

nuScenes-lidarseg : nuScenes-lidarseg is an extension for nuScenes. This dataset has semantic labels of 32 categories and annotates each point from keyframes in nuScenes. We use the 700 scenes in the training set with segmentation labels to fine-tune for the semantic segmentation task, and the 150 scenes in the validation set to verify the performance.

SemanticKITTI : There are 28 semantic classes in SemanticKITTI, and 19 are calculated for evaluation. The annotation cover traffic participants and ground class such as sidewalks. SemanticKITTI contains 22 sequences with only 00-10 annotated. We use the 8th sequence of SemanticKITTI to evaluate the quality of semantic segmentation task and the other 10 sequences for fine-tuning.

We fine-tune our pre-trained model transferring on segmentation on SemanticKITTI, which never shows in the pre-training stage.

KITTI : KITTI is a classical dataset for 3D object detection. It contains 7481 training point clouds and 7518 test point clouds. We follow the official development kit to partition them as training set and validation set. KITTI only evaluates three kinds of objects, including cars, cyclists, and pedestrians. We conduct object detection experiments on the training set of KITTI object detection dataset.

Evaluation Metrics : For fine-tuning on semantic segmentation, we report mIoU and fwIoU validated in specific data. For fine-tuning on object detection, we follow the KITTI (Geiger et al. 2012) comparing methods by mAP: First, we get the AP_R40 (40 recall positions) at an overlap of 0.7 for cars, 0.5 for pedestrians, and 0.5 for cyclists. Then, we compute the average AP over these three classes in the moderately difficult cases.

4.2 Network Architectures

Image Teacher Network: We use a ResNet-50 (He et al. 2016) as our image teacher network. This backbone network is pre-trained with MoCov2 (Chen et al. 2020; He et al. 2020) on ImageNet, enabling our whole training process to get rid of annotations. To maintain the receptive field without reducing the spatial resolution, the second and following stridden convolutions are replaced with dilated convolutions as the same in previous methods (Sautier et al. 2022). The adoption of the dilation strategy enlarges the resolution of the output feature map from $\frac{1}{32}$ to $\frac{1}{4}$ of the input images. Besides, with the upsampling projection layer, the resolution is further recovered to the same as that of input images.

Point Cloud Student Network: Following the common practice as in (Xie et al. 2020; Zhang et al. 2021; Sautier et al. 2022), we adopt the SR-UNet (Choy et al. 2019) as our 3D backbone network, i.e., the student model. SR-UNet has 256 output channels, while image features from the projection layer have 64 channels. We use a fully connected layer after SR-UNet to match the point cloud feature channels with image feature chan-

nels. We quantize the 3D points to voxels as the input of SR-UNet. We generate voxels in Cartesian coordinates with the X-axis range of $[-51.2\text{m}, 51.2\text{m}]$, Y-axis range of $[-51.2\text{m}, 51.2\text{m}]$, and Z-axis range of $[-5.0\text{m}, 3.0\text{m}]$. The voxel size is set as $(0.1\text{m}, 0.1\text{m}, 0.1\text{m})$.

Other Modules: The upsampling projection layer \mathcal{H}^t is composed of a 1×1 convolutional layer and an upsampling layer. The convolutional layer reduces the channels from 2048 to 64. The upsampling layer performs bi-linear interpolation with a scale factor of 4 to adjust the resolution of image features. The projection layer \mathcal{H}^s is a fully-connected layer to align the channels as 64. Besides, the discrete depth size T is set as 118 and the BEV map size is 256×256 .

4.3 Pre-training Details

The 3D network backbone and all the learnable heads are pre-trained on 4 GPUs with a batch size of 16 for 50 epochs. We choose the SGD optimizer with a momentum of 0.9 and a weight decay of 0.0001. This optimizer is also used in all the training of downstream tasks. The initial learning rate is 0.5. A cosine annealing scheduler is employed to adjust the learning rate from the initial value to 0. The temperature hyperparameter in superpixel-to-superpoint contrastive loss and grid-to-grid contrastive loss are all set to 0.07. The coefficients α, β are set to 0.25 and 1, respectively.

Data Augmentation: We apply several augmentations in the pre-training of the backbone. For 3D point clouds, we use random rotation, flip, scale, translate, and drop points that lie in a random cuboid. On the 2D component, we crop and resize to get a patch with the size of $[224, 416]$. Besides, we apply a random horizontal flip, as in SLidR(Sautier et al. 2022). Note that we have to inverse those operations to align the image BEV feature and the point cloud BEV feature.

4.4 Transferring for Semantic Segmentation

In this section, we conduct experiments to transfer the pre-trained backbone for point cloud semantic segmentation. We compare our method with the state-of-the-art approaches on two evaluation protocols, i.e., linear probing and fine-tuning on point clouds semantic segmentation.

Fine-tuning on Semantic Segmentation: We transfer the pre-trained backbone on semantic segmentation by adding a classification head and training them together. We use a linear combination of the cross-entropy and the Lovász Softmax loss (Berman et al. 2018) as our resultant loss. For all the experiments

on semantic segmentation, we fine-tune for 100 epochs with a batch size of 16 and the learning rate is 0.02 in nuScenes. We evaluate performance of semantic segmentation on nuScenes-lidarseg(Caesar et al. 2020) and SemanticKITTI(Behley et al. 2019).

We compare Our HVDistill with SLidR and a few other methods on the few-shot end-to-end semantic segmentation task and show the results in Tab. 1, where 'P-gain' represents the performance improvement of the pretraining method compared to the "Train from Scratch" baseline. We observe that all representation pre-training methods are better than random initialization. In particular, our method performs the best. The *mIoU* is 14.4% and 18.3% higher than random initialization on nuScenes-lidarseg and SemanticKITTI, and 4.4% and 5.1% higher than SLidR on the two datasets.

This proves the advantage of exploiting the hybrid-view features in distilling knowledge from pre-trained image networks. We further evaluate the performance of our method in fine-tuning with different percentages of annotated training data: 1%, 5%, 10%, 25%, and 100%. The results are shown in Tab. 2. Again, our method performs the best. Compared to random initialization, our *mIoU* improvement is 14.4% for 1% annotation, 10.4% for 5% annotation, 6.3% for 10% annotation, 5.3% for 25% annotation, and 2.4% for 100% annotation. These results verify that our approach does provide a better initialization of point cloud networks.

Linear Probing: Next, we evaluate the transferring methods on linear probing.

Here, we add a linear classification head based on the pre-trained 3D backbone. During linear probing, we freeze the backbone and only train the classification head. As in fine-tuning, a linear combination of the cross-entropy and the Lovász-Softmax loss(Berman et al. 2018) are utilized as our loss. We train on nuScenes for 50 epochs with a batch size of 16 on 4 GPUs with 100% of the available annotations. The initial learning rate is 0.05.

The comparison results are summarized in Tab. 4. Among all the methods, ours is again the best performing, with *mIoU* of 39.5%. This again shows that our hybrid-view distillation can learn more discriminative point cloud representations than single-view distillation such as SLidR(Sautier et al. 2022) and PPKT(Liu et al. 2021a).

4.5 Transferring for Few-Shot Object Detection

The object detection task aims to recognize foreground objects from raw data, such as point clouds, which is a fundamental problem in computer vision. Generally, it first uses a backbone to learn representations

Table 1: Performance comparison of different pre-training methods for semantic segmentation by fine-tuning. On nuScenes and SemanticKITTI we use only 1% of the annotated training data, respectively. The results with * are from (Sautier et al. 2022). The results are the $mIoU(\%)$ on the validation sets of nuScenes and SemanticKITTI.

Initialization	nuScenes(Caesar et al. 2020)		SemanticKITTI(Behley et al. 2019)	
	mIoU	P-gain	mIoU	P-gain
Train from scratch	28.3	-	31.4	-
PointContrast*(Xie et al. 2020)	32.5	+4.2	41.1	+9.7
DepthContrast*(Zhang et al. 2021)	31.7	+3.4	41.5	+10.1
PPKT*(Liu et al. 2021a)	37.8	+9.5	43.9	+12.5
SLidR*(Sautier et al. 2022)	38.3	+10.0	44.6	+13.2
HVDistill (Ours)	42.7^{↑4.4}	+14.4	49.7^{↑5.1}	+18.3

Table 2: Performance comparison of random initialization and our pre-trained backbone using our method HVDistill for semantic segmentation with different percentages of annotated training data on nuScenes. The results are the $mIoU(\%)$ on the validation set of nuScenes.

Initialization	1%		5%		10%		25%		100%	
	mIoU	P-gain	mIoU	P-gain	mIoU	P-gain	mIoU	P-gain	mIoU	P-gain
Train from scratch	28.3	-	46.2	-	56.6	-	64.0	-	74.2	-
SLidR(Sautier et al. 2022)	38.3	+10.0	52.2	+6.0	58.8	+2.2	66.2	+1.8	74.6	+0.4
HVDistill (Ours)	42.7^{↑4.4}	+14.4	56.6^{↑4.4}	+10.4	62.9^{↑4.1}	+6.3	69.3^{↑3.5}	+5.3	76.6^{↑2.0}	+2.4

Table 3: Performance comparison of methods for object detection by fine-tuning pre-trained networks using different percentages of the annotated training data in the KITTI. We present the average $mAP(\%)$ of cars, cyclists, and pedestrians in moderately difficult cases.

Initialization	1%	5%	10%	20%
Part-A2(Shi et al. 2021)	0.04	62.3	67.1	70.9
PVRCNN++(Shi et al. 2023)	40.0	66.0	70.1	70.9
Train from scratch	41.7	67.2	69.6	70.8
HVDistill (Ours)	50.4(+8.7)	70.0(+3.0)	70.8(+1.3)	71.9(+1.1)

Table 4: Performance comparison of different pre-training methods for semantic segmentation by linear probing on nuScenes.

Initialization	Linear Prob(mIoU)
Random	6.8
PointContrast*(Xie et al. 2020)	21.9
DepthContrast*(Zhang et al. 2021)	22.1
PPKT*(Liu et al. 2021a)	36.4
SLidR	38.8
HVDistill (Ours)	39.5

from raw data and then translates the necessary attributes of the object bounding boxes from the learned representations. To verify the effectiveness of our pre-train method, we fine-tune a detection network, PointRCNN (Shi et al. 2019), by loading the parameters of the backbone pre-trained with our approach.

We conduct our few-shot object detection based on OpenPCDet(Team 2020). In the toolbox, the backbone of PointRCNN is replaced by the pre-trained network SR U-net, and then trained end-to-end for object detection. We fine-tune the restructured detection network for 80 epochs on 4 GPUs with a batch size of 16. We

Table 5: Ablative experiments of different views to perform contrastive distillation when pre-training. We present the $mIoU(\%)$ of semantic segmentation by fine-tuning pre-trained networks using 1% of the annotated training data in nuScenes. ‘‘Random’’ means this model is randomly initialized and trained from scratch.

Method	image-plane	BEV	mIoU
Random	×	×	28.3
w/o IPV	×	✓	37.8
w/o BEV	✓	×	41.5
HVDistill	✓	✓	42.7

use the default settings in OpenPCDet except that the learning rate is changed to 0.01.

On the validation set of KITTI dataset, we performed an extensive comparison between our pretrained model and the train-from-scratch baseline, utilizing varying percentages of annotated training data. The results of this comparison are delineated in Tab. 3. Once again, our method stands out as the top performer in this evaluation. It is noteworthy that our achieved Mean Average Precision (mAP) surpasses the train-from-scratch with 1% annotated data by a signifi-

cant margin of 8.7%. In addition, we compared our pre-trained model to state-of-the-art (SOTA) 3D detection methods. Our pretrained model consistently demonstrated its superiority over the cutting-edge Part-A2 and PVRCNN++ methods.

4.6 Ablative Experiments

We further conduct ablative experiments to evaluate the design choices in our proposed approach.

Effect of Different Views: We study the effect of different views in our contrastive distillation framework. We compare three networks: (1) train from scratch, (2) HVDistill without BEV distillation, (3) HVDistill without IPV distillation, and (4) HVDistill. After pre-training, we transfer the four backbones on semantic segmentation with 1% annotated training data and test them as in Sec. 4.4.

The results are presented in Tab. 5. The IPV-only (w/o BEV in this table) models achieve 41.5% mIoU, improving the randomly initialized one with 13.2%. The BEV-only (w/o IPV in this table) models achieve 37.8% mIoU, improving the randomly initialized one with 9.5%. Our HVDistill combines both of BEV and IPV, and further boost the performance to 42.7% mIoU, demonstrating the effectiveness of our hybrid-view distillation framework.

A detail comparison in different classes for semantic segmentation in SemanticKITTI is presented in Tab. 6. When comparing our HVDistill to the w/o BEV model, our approach achieves similar or superior performance in almost all classes, except for bicycle, pole, and traffic-sign. These three object classes are thin and extremely challenging to recognize from the bird’s-eye view due to their limited spatial presence and intricate details. The BEV representation may struggle to capture these nuanced characteristics accurately, resulting in decreased recognition and segmentation performance for these classes. However, it’s worth noting that our method using BEV-only features outperforms the w/o BEV model in categories such as other-vehicle, building, and parking. This suggests the effectiveness of BEV contrast distillation, particularly for larger objects, where the BEV view excels. The combination of BEV-based and IPV-based contrast distillation contributes to significant overall improvements, demonstrating that BEV and IPV complement each other effectively. This combined approach offers a promising strategy for 2D-to-3D knowledge transfer in our framework.

Additionally, we did qualitative analysis in Figure 3. The bird-eye view effectively preserves the 3D layout of the scene. In image-plane view distillation, the corre-

spondence between superpoints and superpixels hinges on a projection-based approach. However, this method can introduce a challenge wherein points from varying depths may project to closely situated locations on the image-plane view, potentially leading to the misgrouping of these points into the same cluster, thereby creating ambiguity. As in Figure 3, while points in purple area are clustered as superpoints to represent the left car in the image, it contains both the car (points in black area) and part of ground (points in green area). In contrast, the integration of depth information and the re-projection of pixels into 3D space within the bird-eye view representation alleviates this issue, providing a more accurate representation of the scene.

In addition, the bird-eye view representation offers a mitigation strategy for occlusion and scaling issues, which are notably more complex to resolve in the image-plane view. These inherent advantages are particularly advantageous for the recognition of large objects, as exemplified in Table 6.

Effect of Point Supervision:

We study the effect of point supervision on our HVDistill and present the results in Table 7.

In this table, “w/o point” means predicting the depth distribution for each point without the guidance or the supervision of projected points, “sparse point depth” indicates only the pixels with projected points are transformed to the BEV representation with the depth provided by the corresponding point, “point guided depth distribution” concatenated the sparse depth map provided by projected points and the feature map to predict the depth distribution without extra supervision, and our method devises the depth module with the supervision of projected points to make depth estimation. Among the competitors, our method with projected point supervision achieves the best performance, highlighting the importance of integrating point-supervised depth prediction in image-to-BEV transformation in our HVDistill.

Effect of Scaling Up Pretraining Data: In addition to evaluating the performance of HVDistill, we conduct an experiment to assess the impact of using different portions of nuScenes. We present the evaluated results of semantic segmentation on nuScenes in Table 8 and on SemanticKITTI in Figure 4. The nuScenes training data are divided into subsets representing varying sizes. We observe notable variations in performance when utilizing different portions of the pretraining data. Specifically, we find that larger portions of pretraining data consistently yield improved results compared to smaller or limited subsets of these two datasets. These findings suggest that the inclusion of additional pretraining data

Table 6: Performance comparison of methods for fine-tuning on semantic segmentation with 1% percent of annotated training data on SemanticKITTI. The results are the $mIoU$ (%) on the validation set of SemanticKITTI.

Method	car	bicycle	motorcycle	truck	other-vehicle	person	bicyclist	motorcyclist	road	parking	sidewalk	other-ground	building	fence	vegetation	trunk	terrain	Pole	traffic-sign	mIoU
Random	83.3	0.0	0.0	0.0	0.4	0.0	0.0	0.0	80.0	0.0	58.8	0.0	76.0	27.4	81.3	33.5	65.0	38.8	21.9	29.8
w/o IPV	91.3	2.8	17.4	20.0	11.9	29.5	28.3	0.0	88.6	25.4	71.4	0.0	86.3	35.5	82.7	57.4	67.5	60.9	43.2	43.2
w/o BEV	94.4	11.7	24.2	30.8	8.4	47.6	45.6	0.0	89.1	24.1	72.8	0.0	85.8	37.9	84.6	59.4	71.2	62.5	47.8	47.3
HVDistill	94.5	6.4	36.8	49.3	16.2	47.4	47.5	0.0	90.9	28.9	74.8	0.1	88.6	46.3	85.5	62.1	71.0	60.7	45.5	50.1

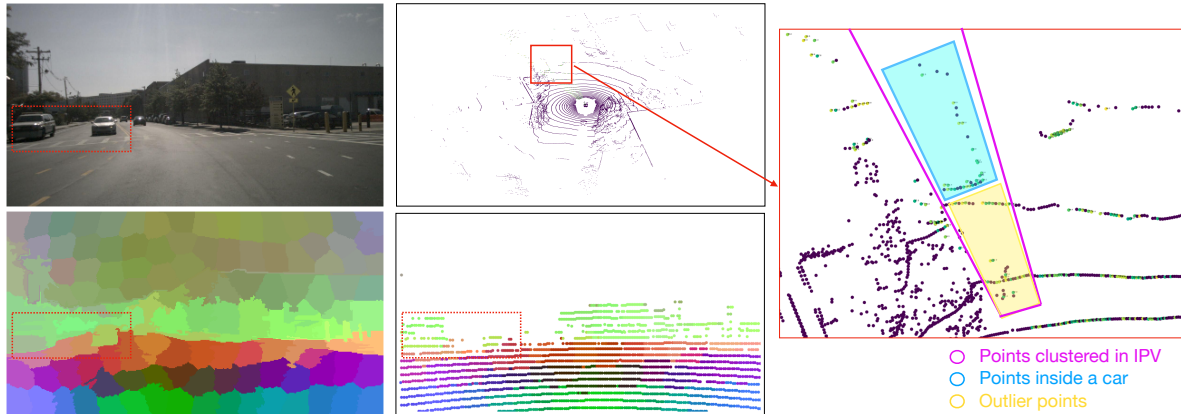


Fig. 3: The figure shows the raw image and superpixels on the left, point clouds in BEV view and superpoints on the middle, and The zoomed-out image focuses on the superpoints surrounding the selected car on the right. Points in the red boxes represent the same area. While points in purple are clustered as superpoints to represent the left car in the image, it contains not only the car (points in black area) but also part of ground (points in green area), introducing ambiguity for points.

Table 7: Ablative experiments of different design choices to build BEV features. We present the mIoU of semantic segmentation by fine-tuning pre-trained networks using 1% of the annotated training data in nuScenes.

Method	mIoU
w/o point	39.6
sparse point depth	41.2
Point guidance depth prediction	42.2
HVDistill	42.7

has the potential to further enhance the performance of our proposed method. With the availability of a larger dataset, we anticipate even more substantial gains in feature extraction.

The Effect of Pretrained Image Teacher: To explore the influence of different image teachers on our proposed method, we conduct experiments utilizing multiple pre-trained image teachers in addition to the MoCoV2. The results are presented in Table 9. Surprisingly, Despite DINO’s (Caron et al. 2021) superior performance in image classification, this image teacher network is not optimally suited for our HVDistill. These

Table 8: Performance of different training data for semantic segmentation by fine-tuning on nuScenes. We use 1% training data for fine-tuning.

Data for pretraining	mIoU	fwIoU
5%	35.7	72.3
20%	38.9	75.0
50%	41.2	76.7
100%	42.7	77.1

Table 9: Performance comparison of our method with different image teachers for semantic segmentation by fine-tuning on nuScenes. We use 1% training data for fine-tuning.

Teacher method	top-1 acc(ImageNet)	mIoU	fwIoU
Dino	75.3	41.4	77.0
Supervised	79.3	42.9	77.2
MoCoV2	71.1	42.7	77.1

results suggest that the choice of pre-trained image teacher should be carefully considered, taking into account its compatibility with the target task. While some

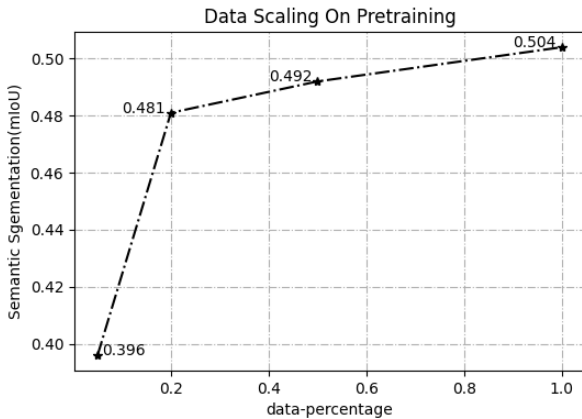


Fig. 4: Performance of different training data for semantic segmentation by fine-tuning on SemanticKITTI. We use 1% training data for fine-tuning.

Table 10: Performance comparison of different contrast learning methods on IPV branch. We use 1% training data of nuScenes for fine-tuning on semantic segmentation.

contrast method on IPV branch	mIoU	fwIoU
None	33.4	71.8
pixel-to-point	41.1	76.8
Superpixel-to-superpoint	42.7	77.1

image teachers may excel in certain domains, their performance may not necessarily translate directly to improve results in other tasks.

Comparison of image-plane-view Method: We explore pixel-to-point and superpixel-to-superpoint contrast learning methods on IPV branch in Table 10. The pixel-to-point contrast learning involves computing at individual pixel and corresponding point, while superpixel-to-superpoint contrast learning aggregates visually similar pixels and translates knowledge in superpixel level. Our results show that the pixel-to-point does yield a lower performance, as the noise of calibration of LiDAR and camera led to suboptimal results.

Ablation study of α and β : In Tab.4, we present the mIoU scores achieved with different weight ratios, specifically $\alpha : \beta$. We varied these ratios while keeping β constant and observed the corresponding performance changes. The table highlights the following findings: When $\alpha : \beta$ is set to 1:1, the performance reaches its lowest point, indicating that an equal contribution from both image-plane view and bird’s-eye view distillation has a minimal impact on performance. The best performance is achieved when $\alpha : \beta$ is set to 4:1, underscoring the significance of the bird’s-eye view distillation in enhancing semantic segmentation. We note that

Table 11: Ablation of α and β . $\alpha : \beta = 4:1$ is the best choice.

$\alpha : \beta$	mIoU
4 : 1	50.1
2 : 1	49.8
1 : 1	49.4
1 : 2	49.5

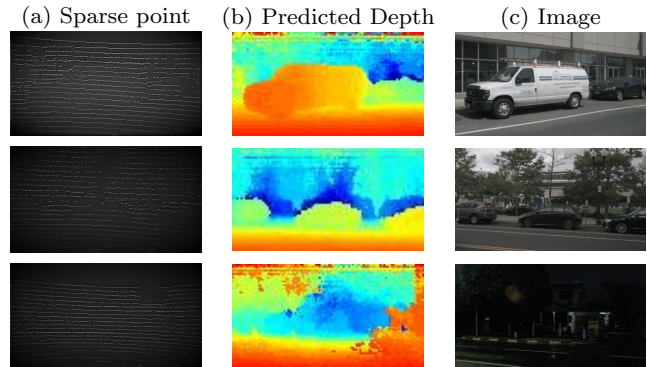


Fig. 5: Visualization of the predicted depth of different objects. With sparse point cloud supervision, image features can predict the dense depth and preserve geometric information. Each row represents a specific scene.

while there is variation in performance across different weight settings, the impact on overall performance is relatively minimal.

4.7 Qualitative Results

Visualization of predicted depth: We visualize the discrete depth predictions obtained from our model in Figure 5, which represent the depth value with the maximum probability for each pixel. We have also included a comparison with sparse depth information derived from point clouds. The results demonstrate that our model performs well in diverse scenes, including both daytime and nighttime scenarios, and can accurately predict depth for a wide range of objects, such as cars and trees. Overall, our approach shows promising results for depth estimation in real-world settings.

Visualization of Semantic segmentation results: Figure 6 illustrates the semantic segmentation results on the nuScenes validation set, including (a) Ground Truth, (b) Train from scratch, (c) SLiDR, and (d) Our method. Our model can predict accurate class for distant and highly occluded objects, demonstrating the high-quality predictions of our model.

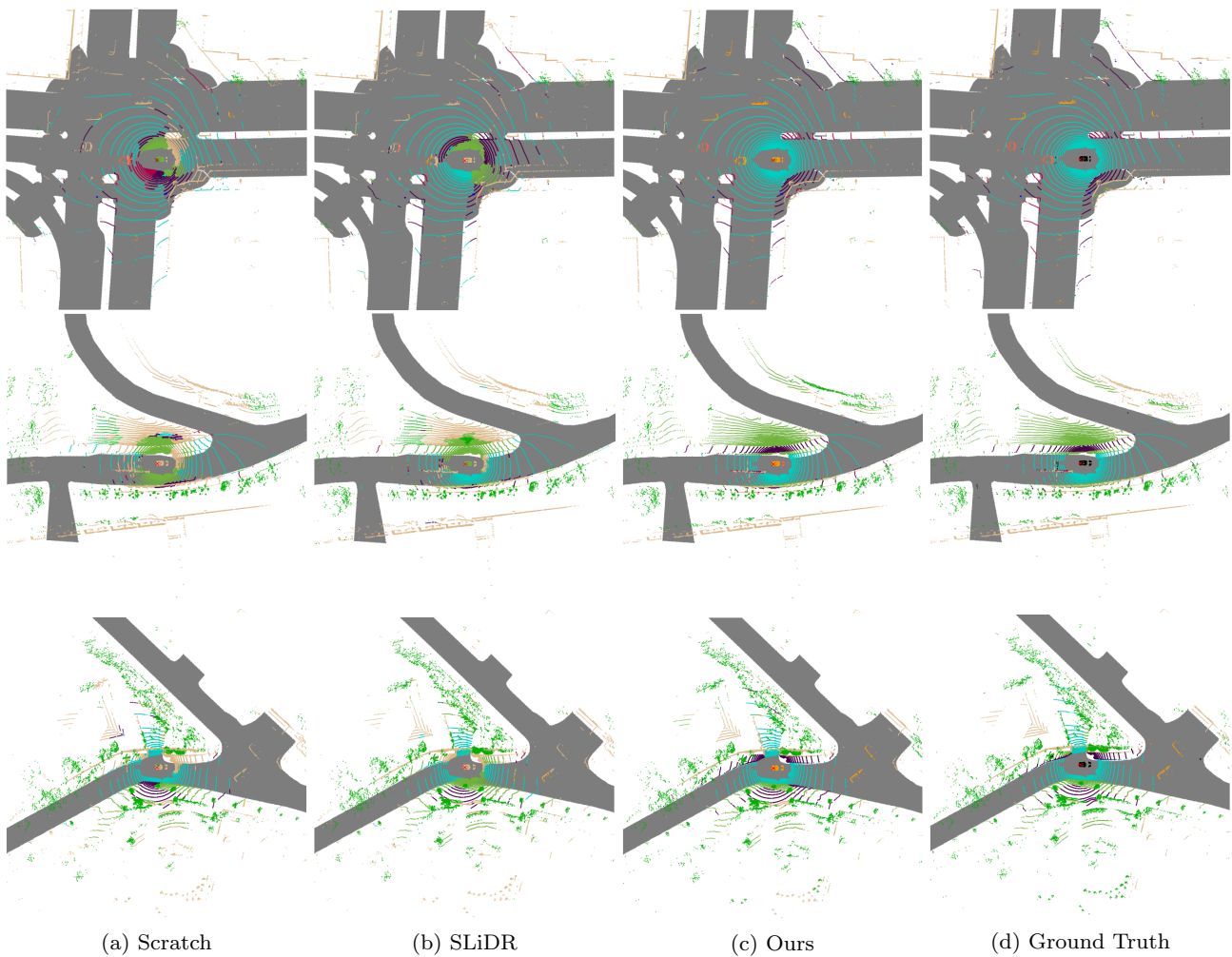


Fig. 6: Qualitative results of 3D semantic segmentation on the nuScenes validation set.

5 Conclusion

In this paper, we propose HVDistill, a self-supervised 2D-to-3D distillation method to transfer knowledge from a pre-trained image model to a point cloud neural network via two cross-modality contrastive losses, one from the image plane view (IPV) and the other from BEV. The BEV contrastive distillation utilizes the depth information in the point clouds to preserve the geometric information, providing a complement for the mainstream IPV contrastive distillation. The experiments demonstrate that our pre-train method brings significant improvement in downstream tasks compared to the state-of-the-art. We believe that our method takes a step towards more effective knowledge transfer between modalities.

Data availability: The nuScenes (Caesar et al. 2020) dataset and nuScenes-lidarseg (Caesar et al. 2020) dataset can be obtained from <https://www.nuscenes.org/>.

The KITTI (Geiger et al. 2012) dataset and SemanticKITTI (Behley et al. 2019) dataset can be obtained from <https://www.cvlibs.net/datasets/kitti/>. The code that supports the findings of this study are available from the corresponding author, Yanyong Zhang, upon reasonable request.

Declarations

Conflict of interest There are no conflicts to declare.

References

- Achanta R, Shaji A, Smith K, Lucchi A, Fua P, Süsstrunk S (2012) Slic superpixels compared to state-of-the-art superpixel methods. *IEEE transactions on pattern analysis and machine intelligence (TPAMI)* 34(11):2274–2282 5
- Alexiou E, Yang N, Ebrahimi T (2020) Pointxr: A toolbox for visualization and subjective evaluation of point clouds in virtual reality. In: 2020 Twelfth International Conference

- on Quality of Multimedia Experience (QoMEX), IEEE, pp 1–6 [1](#)
- Alwassel H, Mahajan D, Korbar B, Torresani L, Ghanem B, Tran D (2020) Self-supervised learning by cross-modal audio-video clustering. *Advances in Neural Information Processing Systems (NeurIPS)* 33:9758–9770 [3](#)
- Behley J, Garbade M, Milioto A, Quenzel J, Behnke S, Stachniss C, Gall J (2019) Semantickitti: A dataset for semantic scene understanding of lidar sequences. In: *Proceedings of the IEEE/CVF International Conference on Computer Vision (ICCV)*, pp 9297–9307 [1](#), [3](#), [7](#), [8](#), [9](#), [13](#)
- Berman M, Triki AR, Blaschko MB (2018) The lovász-softmax loss: A tractable surrogate for the optimization of the intersection-over-union measure in neural networks. In: *Proceedings of the IEEE conference on computer vision and pattern recognition (CVPR)*, pp 4413–4421 [8](#)
- Bucilua C, Caruana R, Niculescu-Mizil A (2006) Model compression. In: *Proceedings of the 12th ACM SIGKDD international conference on Knowledge discovery and data mining (SIGKDD)*, pp 535–541 [3](#)
- Caesar H, Bankiti V, Lang AH, Vora S, Liong VE, Xu Q, Krishnan A, Pan Y, Baldan G, Beijbom O (2020) nuscenes: A multimodal dataset for autonomous driving. In: *Proceedings of the IEEE/CVF conference on computer vision and pattern recognition (CVPR)*, pp 11621–11631 [1](#), [3](#), [7](#), [8](#), [9](#), [13](#)
- Caron M, Touvron H, Misra I, Jégou H, Mairal J, Bojanowski P, Joulin A (2021) Emerging properties in self-supervised vision transformers. In: *Proceedings of the IEEE/CVF international conference on computer vision (ICCV)*, pp 9650–9660 [11](#)
- Chen H, Luo S, Gao X, Hu W (2021) Unsupervised learning of geometric sampling invariant representations for 3d point clouds. In: *Proceedings of the IEEE/CVF International Conference on Computer Vision (ICCV)*, pp 893–903 [3](#)
- Chen S, Duan C, Yang Y, Li D, Feng C, Tian D (2019) Deep unsupervised learning of 3d point clouds via graph topology inference and filtering. *IEEE transactions on image processing (TIP)* 29:3183–3198 [3](#)
- Chen X, Fan H, Girshick R, He K (2020) Improved baselines with momentum contrastive learning. *arXiv preprint arXiv:200304297* [7](#)
- Cho JH, Hariharan B (2019) On the efficacy of knowledge distillation. In: *Proceedings of the IEEE/CVF international conference on computer vision (ICCV)*, pp 4794–4802 [3](#)
- Choy C, Gwak J, Savarese S (2019) 4d spatio-temporal convnets: Minkowski convolutional neural networks. In: *Proceedings of the IEEE/CVF Conference on Computer Vision and Pattern Recognition (CVPR)*, pp 3075–3084 [7](#)
- Duan Y, Peng J, Zhang Y, Ji J, Zhang Y (2022) Pfilter: Building persistent maps through feature filtering for fast and accurate lidar-based slam. In: *2022 IEEE/RSJ International Conference on Intelligent Robots and Systems (IROS)*, IEEE, pp 11087–11093 [1](#)
- Geiger A, Lenz P, Urtasun R (2012) Are we ready for autonomous driving? the kitti vision benchmark suite. In: *2012 IEEE conference on computer vision and pattern recognition (CVPR)*, IEEE, pp 3354–3361 [3](#), [7](#), [13](#)
- Grill JB, Strub F, Altché F, Tallec C, Richemond P, Buchatskaya E, Doersch C, Avila Pires B, Guo Z, Gheshlaghi Azar M, et al. (2020) Bootstrap your own latent: a new approach to self-supervised learning. *Advances in neural information processing systems (NeurIPS)* 33:21271–21284 [2](#)
- Guo X, Shi S, Wang X, Li H (2021) Liga-stereo: Learning lidar geometry aware representations for stereo-based 3d detector. In: *Proceedings of the IEEE/CVF International Conference on Computer Vision (CVPR)*, pp 3153–3163 [3](#), [5](#)
- Gupta S, Hoffman J, Malik J (2016) Cross modal distillation for supervision transfer. In: *Proceedings of the IEEE conference on computer vision and pattern recognition (CVPR)*, pp 2827–2836 [3](#), [5](#)
- Han B, Ma JW, Leite F (2021a) A framework for semi-automatically identifying fully occluded objects in 3d models: Towards comprehensive construction design review in virtual reality. *Advanced Engineering Informatics* 50:101398 [1](#)
- Han Z, Shang M, Liu YS, Zwicker M (2019a) View inter-prediction gan: Unsupervised representation learning for 3d shapes by learning global shape memories to support local view predictions. In: *Proceedings of the AAAI conference on artificial intelligence (AAAI)*, vol 33, pp 8376–8384 [3](#)
- Han Z, Wang X, Liu YS, Zwicker M (2019b) Multi-angle point cloud-vae: Unsupervised feature learning for 3d point clouds from multiple angles by joint self-reconstruction and half-to-half prediction. In: *2019 IEEE/CVF International Conference on Computer Vision (ICCV)*, IEEE, pp 10441–10450 [3](#)
- Han Z, Wang X, Liu YS, Zwicker M (2021b) Hierarchical view predictor: Unsupervised 3d global feature learning through hierarchical prediction among unordered views. In: *Proceedings of the 29th ACM International Conference on Multimedia (ACM MM)*, pp 3862–3871 [3](#)
- He K, Zhang X, Ren S, Sun J (2016) Deep residual learning for image recognition. In: *Proceedings of the IEEE conference on computer vision and pattern recognition (CVPR)*, pp 770–778 [7](#)
- He K, Fan H, Wu Y, Xie S, Girshick R (2020) Momentum contrast for unsupervised visual representation learning. In: *Proceedings of the IEEE/CVF conference on computer vision and pattern recognition (CVPR)*, pp 9729–9738 [2](#), [5](#), [7](#)
- He K, Chen X, Xie S, Li Y, Dollár P, Girshick R (2022) Masked autoencoders are scalable vision learners. In: *Proceedings of the IEEE/CVF Conference on Computer Vision and Pattern Recognition (CVPR)*, pp 16000–16009 [2](#)
- Hinton G, Vinyals O, Dean J, et al. (2015) Distilling the knowledge in a neural network. *arXiv preprint arXiv:150302531* 2(7) [3](#)
- Huang J, Huang G, Zhu Z, Du D (2021) Bevdet: High-performance multi-camera 3d object detection in bird-eye-view. *arXiv preprint arXiv:211211790* [3](#)
- Jiang J, Lu X, Ouyang W, Wang M (2021) Unsupervised representation learning for 3d point cloud data. *arXiv preprint arXiv:211006632* [3](#), [5](#)
- Li CL, Zaheer M, Zhang Y, Póczos B, Salakhutdinov R (2018) Point cloud gan. *arXiv preprint arXiv:181005795* [3](#)
- Li Y, Deng J, Zhang Y, Ji J, Li H, Zhang Y (2022a) Ezfusion: A close look at the integration of lidar, millimeter-wave radar, and camera for accurate 3d object detection and tracking. *IEEE Robotics and Automation Letters (RAL)* 7(4):11182–11189 [1](#)
- Li Z, Wang W, Li H, Xie E, Sima C, Lu T, Qiao Y, Dai J (2022b) Bevformer: Learning bird’s-eye-view representation from multi-camera images via spatiotemporal transformers. In: *Computer Vision—ECCV 2022: 17th European Conference, Tel Aviv, Israel, October 23–27, 2022, Proceedings, Part IX*, Springer, pp 1–18 [3](#)

- Liu YC, Huang YK, Chiang HY, Su HT, Liu ZY, Chen CT, Tseng CY, Hsu WH (2021a) Learning from 2d: Contrastive pixel-to-point knowledge transfer for 3d pretraining. arXiv preprint arXiv:210404687 [2](#), [4](#), [8](#), [9](#)
- Liu Z, Qi X, Fu CW (2021b) 3d-to-2d distillation for indoor scene parsing. In: Proceedings of the IEEE/CVF Conference on Computer Vision and Pattern Recognition (CVPR), pp 4464–4474 [3](#), [5](#)
- Liu Z, Tang H, Amini A, Yang X, Mao H, Rus D, Han S (2022) Bevfusion: Multi-task multi-sensor fusion with unified bird's-eye view representation. arXiv preprint arXiv:220513542 [3](#)
- Mirzadeh SI, Farajtabar M, Li A, Levine N, Matsukawa A, Ghasemzadeh H (2020) Improved knowledge distillation via teacher assistant. In: Proceedings of the AAAI conference on artificial intelligence (AAAI), vol 34, pp 5191–5198 [3](#)
- Oord Avd, Li Y, Vinyals O (2018) Representation learning with contrastive predictive coding. arXiv preprint arXiv:180703748 [5](#), [6](#)
- Qi X, Wang W, Yuan M, Wang Y, Li M, Xue L, Sun Y (2020) Building semantic grid maps for domestic robot navigation. International Journal of Advanced Robotic Systems 17(1):1729881419900066 [1](#)
- Rao Y, Lu J, Zhou J (2020) Global-local bidirectional reasoning for unsupervised representation learning of 3d point clouds. In: Proceedings of the IEEE/CVF Conference on Computer Vision and Pattern Recognition (CVPR), pp 5376–5385 [3](#)
- Sanghi A (2020) Info3d: Representation learning on 3d objects using mutual information maximization and contrastive learning. In: European Conference on Computer Vision (ECCV), Springer, pp 626–642 [3](#)
- Sautier C, Puy G, Gidaris S, Boulch A, Bursuc A, Marlet R (2022) Image-to-lidar self-supervised distillation for autonomous driving data. In: Proceedings of the IEEE/CVF Conference on Computer Vision and Pattern Recognition (CVPR), pp 9891–9901 [2](#), [4](#), [5](#), [7](#), [8](#), [9](#)
- Shi S, Wang X, Li H (2019) Pointcnn: 3d object proposal generation and detection from point cloud. In: Proceedings of the IEEE/CVF conference on computer vision and pattern recognition (CVPR), pp 770–779 [9](#)
- Shi S, Wang Z, Shi J, Wang X, Li H (2021) From points to parts: 3d object detection from point cloud with part-aware and part-aggregation network. IEEE Trans Pattern Anal Mach Intell 43(8):2647–2664 [9](#)
- Shi S, Jiang L, Deng J, Wang Z, Guo C, Shi J, Wang X, Li H (2023) Pv-rcnn++: Point-voxel feature set abstraction with local vector representation for 3d object detection. International Journal of Computer Vision (IJCV) 131(2):531–551 [1](#), [9](#)
- Team OD (2020) Openpcdet: An open-source toolbox for 3d object detection from point clouds. <https://github.com/open-mmlab/OpenPCDet> [9](#)
- Tian Y, Krishnan D, Isola P (2019) Contrastive representation distillation. arXiv preprint arXiv:191010699 [3](#)
- Wang PS, Yang YQ, Zou QF, Wu Z, Liu Y, Tong X (2021) Unsupervised 3d learning for shape analysis via multi-resolution instance discrimination. In: Proceedings of the AAAI Conference on Artificial Intelligence (AAAI), vol 35, pp 2773–2781 [3](#), [5](#)
- Wang Y, Chao WL, Garg D, Hariharan B, Campbell M, Weinberger KQ (2019) Pseudo-lidar from visual depth estimation: Bridging the gap in 3d object detection for autonomous driving. In: Proceedings of the IEEE/CVF Conference on Computer Vision and Pattern Recognition (CVPR), pp 8445–8453 [3](#)
- Wang Y, Mao Q, Zhu H, Deng J, Zhang Y, Ji J, Li H, Zhang Y (2023) Multi-modal 3d object detection in autonomous driving: a survey. International Journal of Computer Vision (IJCV) pp 1–31 [1](#)
- Xiao T, Liu S, De Mello S, Yu Z, Kautz J, Yang MH (2022) Learning contrastive representation for semantic correspondence. International Journal of Computer Vision (IJCV) 130(5):1293–1309 [2](#)
- Xie J, Zhan X, Liu Z, Ong YS, Loy CC (2022) Delving into inter-image invariance for unsupervised visual representations. International Journal of Computer Vision (IJCV) 130(12):2994–3013 [2](#)
- Xie S, Gu J, Guo D, Qi CR, Guibas L, Litany O (2020) Point-contrast: Unsupervised pre-training for 3d point cloud understanding. In: European conference on computer vision (ECCV), Springer, pp 574–591 [2](#), [3](#), [7](#), [9](#)
- Yang Y, Feng C, Shen Y, Tian D (2017) Foldingnet: Interpretable unsupervised learning on 3d point clouds. arXiv preprint arXiv:171207262 2(3):5 [3](#)
- Zhang L, Ma K (2020) Improve object detection with feature-based knowledge distillation: Towards accurate and efficient detectors. In: International Conference on Learning Representations (ICLR) [3](#)
- Zhang Z, Girdhar R, Joulin A, Misra I (2021) Self-supervised pretraining of 3d features on any point-cloud. In: Proceedings of the IEEE/CVF International Conference on Computer Vision (ICCV), pp 10252–10263 [3](#), [7](#), [9](#)
- Zhao B, Cui Q, Song R, Qiu Y, Liang J (2022a) Decoupled knowledge distillation. In: Proceedings of the IEEE/CVF Conference on Computer Vision and Pattern Recognition (CVPR), pp 11953–11962 [3](#)
- Zhao Y, Fang G, Guo Y, Guibas L, Tombari F, Birdal T (2022b) 3dpointcaps++: Learning 3d representations with capsule networks. International Journal of Computer Vision (IJCV) 130(9):2321–2336 [3](#)
- Zhu H, Deng J, Zhang Y, Ji J, Mao Q, Li H, Zhang Y (2022) Vpfnnet: Improving 3d object detection with virtual point based lidar and stereo data fusion. IEEE Transactions on Multimedia (TMM) [1](#)